buildings

MDPI

Article

Laboratory Test Study on Pile Jacking Penetration Mechanism Considering Different Diameter and Length Based on Photoelectric Integration Technology

Lifeng Wang [1], Shuo Zhang [2], Shiqiang Li [3], Jun Wang [3], Xunlong Niu [3], Donglei Wang [4,5] and Yonghong Wang [2,*]

[1] Qingdao Fangshuo Construction Technology Co., Ltd., Qingdao 266000, China
[2] School of Civil Engineering, Qingdao University of Technology, Qingdao 266033, China
[3] China State Construction Zhongxin Construction Engineering Co., Ltd., Qingdao 266033, China
[4] Qingdao Green Technology Geotechnical Engineering Co., Ltd., Qingdao 266033, China
[5] Qingdao Yongyuan Marine Technology Co., Ltd., Qingdao 266033, China
* Correspondence: hong7986@163.com

Abstract: Model tests are carried out on the jacked single piles of different diameters and pile lengths under the model pile of different diameters and pile lengths in clayey soil, which aims to investigate the penetration mechanical mechanism. How to accurately test the pile end resistance and pile side resistance during jacked pile sinking is particularly important. In this paper, a full-section spoke-type pressure sensor, a double diaphragm temperature self-compensating fiber Bragg grating (FBG) earth pressure sensor and a sensitized miniature FBG strain sensor are jointly applied to a single pile penetration model test to test a single pile driving force, pile end resistance and pile body stress during penetration. The test results show that the load transfer performance of test piles will be affected by different diameters, and the axial force transfer capability of a large diameter in the depth direction is better than that of a small diameter since the compacting effect is more obvious. The unit skin friction of the pile increases gradually as the depth increases, which is larger due to the lateral extrusion force increasing as the diameter increases. At the same depth, the unit skin friction of two different diameter piles demonstrates "friction fatigue", which also decreases obviously as the depth increases. Under the conditions of this test, the maximum frictional resistance of the pile TP1 pile side is about 27.7% higher than that of the test pile TP2. In the static pile sinking process of three test piles in cohesive soil, 50% is end bearing; therefore, there is 50% friction, and the diameter influences the end bearing and the length influences the friction.

Keywords: FBG sensor; spoke type pressure sensor; static pile; force state

Citation: Wang, L.; Zhang, S.; Li, S.; Wang, J.; Niu, X.; Wang, D.; Wang, Y. Laboratory Test Study on Pile Jacking Penetration Mechanism Considering Different Diameter and Length Based on Photoelectric Integration Technology. *Buildings* **2023**, *13*, 1247. https://doi.org/10.3390/buildings13051247

Academic Editors: Suraparb Keawsawasvong and Erwin Oh

Received: 14 February 2023
Revised: 29 March 2023
Accepted: 6 April 2023
Published: 9 May 2023

1. Introduction

Jacked piles are used frequently in soft soil regions of China, including Guangdong, Zhejiang, and Shanghai as well as some pile foundation projects in the Qingdao region due to their high bearing capacity, simplicity of construction, quick construction speed, and lack of vibration and noise during construction. [1,2]. The force condition of piles during static pile sinking has been extensively studied over the years utilizing theoretical analysis, field measurements, indoor experiments, and numerical simulations, and various research findings have been attained. [3–14]. In terms of theoretical analysis, Jingpei Li et al. [3] enhanced the Cambridge model by computing the pile side resistance and end resistance using the column bore expansion theory and the SMP criterion-based spherical bore expansion theory, fully validating their results with examples. Saga set et al. [4] provided analytical methods for columnar expansion in infinite incompressible fluids to address huge strain issues in plastic and elastic zones. I Field measurements were carried out by Zhang Mingyi et al. [5], who installed homemade pressure transducers at the pile end and applied resistance strain gauges to the pile body, respectively. They

then compared the measured compression force and piled lateral frictional resistance with the static touch curves and talked about the residual stresses at the pile end. Ma Hailong et al. [6] completed in situ static pile sinking tests of open and closed model piles in soft soil areas and compared their bearing capacity magnitude relationships from the perspective of timeliness. Kou Hailey et al. [7,8] monitored the pile side resistance and end resistance development of five full-scale open-ended PHC pipe piles that penetrated the layered foundation utilizing pre-buried fiber-optic grating sensors in the pile body. She investigated the variation of mechanical properties, such as the bearing capacity of open-ended PHC piles with resting time by using static compression tests with interval time. Given the complex engineering geological conditions, costly capital, complex and variable soil layers, and various uncertainties in the field tests, many scholars explored the force state during the sinking of hydrostatic piles by simplifying the difficult soil conditions in the field and through indoor scaled-down tests or centrifugal model tests. The indoor sinking pile model test is the most direct method to study the mechanical mechanism of hydrostatic pile penetration, and many scholars at home and abroad have studied the problem of hydrostatic pile immersion through indoor model tests. The above research has important theoretical significance, but there are still few model tests of hydrostatic sinking piles in clayey soil layers. Li, Y. N. et al. [9] investigated the distribution of pile-side frictional resistance of stainless steel closed-ended square piles in cohesive soils during static pile driving under different gravity fields with a drum-and-wheel centrifuge from the University of Western Australia. Using a centrifuge, Nicola et al. [10] examined the force performance of model piles on uniform sand soils under dynamic and static loads. They obtained a single curve of the end-bearing response. A new technique for installing piles called the Jacking and Rotary method was presented by Hassan Nor Syamira et al. [11], to determine the behavior of piles tested by static load and compared with their test results by the common method, which is Jacking (J). The findings demonstrate that the J&R method may be used to lay pile foundations, ensuring its use in engineering practice. Model piles of reconstituted calcareous and siliceous sands were tested inside by C. Y. Lee et al. [12] to examine the variables affecting the degradation of pile lateral friction resistance under static and cyclic loading. According to the study's findings, there was a connection between the particles' grade and compressibility. An experimental investigation on the jacking piles' penetrating properties in sandy soils was done by Tautvydas Statkus [13]. On model piles, tests were conducted with five separate dead and variable load components. The link between the pile top displacement and the number of loading cycles was examined after applying 50 loading cycles of load variation. You Wang et al. [14] presented an analytical approach to assess the bearing capacity of jacked piles in cohesive soils. Through parametric analysis, it was determined how certain factors, such as in situ overconsolidation rate, affected the pile's long-term bearing behavior. The findings demonstrate that the suggested approach can forecast the jacked piles' short-term setup and obtain appropriate long-term bearing behavior. The long-term load–displacement curve of the pile is significantly influenced by three soil strength and stiffness factors. Currently, most indoor model experiments are centered on a single component and how the foundation soil layer, different pile lengths, diameters, and end forms impact the pile load transfer law during pile jacking [15,16]. The effect of various pile lengths and diameters on the force state of the sinking process of pile jacking in the same model test is less frequently taken into account. Due to limitations, Sandy soils were mainly chosen for the model test foundation layer, but the engineering pipe piles were not considered primarily applied in the cohesive ground foundation. Many indoor static pile-sinking tests use traditional strain gauge test elements, susceptible to environmental effects, low survival rates, complex construction, and low reliability [17,18]. The fiber grating is a brand-new test element that was created in recent years. Due to its high sensitivity, high resolution, long-term stability, strong anti-interference, waterproof and moisture-proof nature, small size, light weight, and other characteristics, it has gradually replaced the traditional test element and is becoming more and more popular with the general public. It is also used extensively in real-world

engineering and model testing [19–21]. To look into the issue of minor displacements in big model testing, Yong Li et al. [19] used FBG sensors in model tests. The test findings revealed that the FBG sensors have superior measurement precision compared to other traditional sensors, such as strain gauges and micro expansion gauges. A fiber Bragg grating (FBG)-based soil strain measuring technique was put out by RunzhouYou et al. [20]. Field testing was also conducted, and the results showed the measurement's efficacy and reliability and the sensor's high sensitivity to soil strain. Additionally, many FBG soil strain sensors may be deployed on a single fiber even if they have varied center wavelengths, considerably simplifying installation and operation. Zhu Youqun et al. [21] applied FBG and BOTDA jointly to the strain monitoring of the pile body during model test pile sinking.

In this paper, the FBG strain sensor, the FBG pressure sensor and the self-made aluminum model pile are used to install the FBG strain sensor on the pile body using the grooving method and the FBG pressure sensor on the top of the pile and by monitoring the strain and top pressure of the pile body through two sensors. The changes of the pile end resistance, side friction resistance, unit side friction resistance and axial force of the pile body during the static pressure penetration of model piles with pile diameters of 140 and 100 mm and pile lengths of 1200 and 1000 mm were studied.

2. Test Preparation

The test was conducted at Qingdao University of Technology's Electric Control Experiment Center. The instrument for the testing was a large-scale model test system developed by the institution.

2.1. Test System

A data acquisition device, a loading apparatus, and a model box were prepared for the test. Data acquisition mainly includes pile compression, pile end resistance, and axial force. The primary instruments include FS2200RM fiber-optic grating demodulator and DH3816N static strain collector. The loading apparatus mainly comprises the electric control system, hydraulic jack, beam, counterforce frame, static load control system, etc. The electric control system controls the front and rear movement of the loading beam and the hydraulic jack's left and right movement to realize the test pipe pile's static pile sinking process. To directly investigate the process of pile jacking, a tempered glass window was installed on the side of the box body with dimensions of 3 m × 3 m × 2 m, which is part of the indoor model test system. Figure 1 shows the test loading apparatus.

2.2. Test Soil Samples

A Qingdao residential project site provided the soil samples utilized for the indoor model experiments and belonged to the powder clay layer. After transporting the on-site soil samples to the school test site, they were filled in layers, compacted, vibrated, and sprinkled with water to cover the film for about 30 d to be ready for testing [22]. Among them, the site foundation soil is shown in Figure 2. The photo in Figure 2 shows the topmost topsoil of the soil extraction site, and the actual test uses soil 2~3 m below the surface. The measures taken by vibration compaction in this test are to lay wooden boards on the soil after layered filling and compaction, and vibrate on the wooden boards.

Soil samples were taken from the model box, and geotechnical tests were conducted before pile jacking. According to the triaxial test and CD method, the internal friction angle and cohesion details of the site soil layer were obtained [23]. Table 1 lists the pertinent parameters.

Figure 1. Test loading apparatus.

Figure 2. Site foundation soil.

Table 1. Parameters of soil samples.

Relative Density d_s	Weight Density γ/(kN/m^3)	Moisture Content w/%	Liquid Limit w_L/%	Plastic Limit w_p/%	Plasticity Index I_p/%	Cohesion c/kPa	Internal Friction Angle φ/(°)	Modulus of Compression $E_{s1\text{-}2}$/MPa
2.73	18.0	34.8	34.8	21.2	13.6	14.4	8.6	3.3

2.3. Introduction of Model Pile

Three model piles were tested by static compression. The test piles were designed as 1000 mm, while TP1 was 1200 mm with the spoke sensors at the pile end. Hexagonal bolts hold three test piles to the pipe pile's pile end. Table 2 lists the parameters of piles. The tested piles are shown in Figure 3.

Table 2. Model pipe pile parameters.

No.	External Diameter/mm	Pile Length/mm	Pipe Thickness/mm	Form of Pipe End	Elasticity Modulus/GPa	Poisson's Ratio
TP1	140	1200	3	close	72	0.3
TP2	140	1000	3	close	72	0.3
TP3	100	1000	3	close	72	0.3

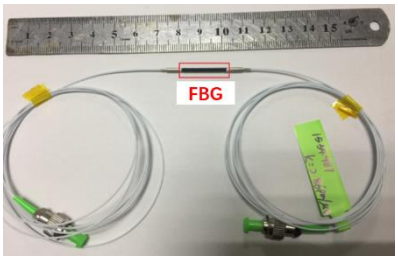

Figure 3. Sensitized miniature FBG sensor.

3. Introduction of Model Sensor

3.1. Sensitized Microfiber Sensing

FBG (fiber-optic grating) sensors are frequently utilized in engineering practices originating of their small size, low impact by the external environment, and easy installation. The sensitized miniature fiber grating sensor, or FBG sensor, used in the test is called the JMFSS-04, which the Shenzhen Jemetech Technology Company designed. It is primarily made up of a fiber grating, clamping sleeve, pigtail, and FC connector. Table 3 displays some specific FBG sensor parameters.

Table 3. Parameters of sensors.

Parameter Type	Wavelength Interval/nm	Central Wavelength/nm	Range/με	Resolution Ratio/με	Usage Temperature/(°C)
numerical value	±3	1510~1590	±1500	1	−30~120

3.2. FBG Fiber-Optic Sensing Principle

The FBG sensor, because of its small size and high sensitivity, the installation slot, FC connector, and the demodulator wiring port need to be scrubbed clean using alcohol and cotton balls before use. Sensor pigtail and fiber grating are connected by fusion in the process of installation alignment to avoid excessive pulling, resulting in the detachment of the pigtail and fiber grating, affecting the survival rate of the FBG sensor. The fiber grating must be pre-stretched when pasting the fixed sensor to increase its pressure range.

The strain variation value can be calculated from the wavelength difference $\Delta\lambda_B$ of the fiber as follows.

$$\Delta\lambda_B = (1 - P_e)\lambda_B\Delta\varepsilon = K_\varepsilon\Delta\varepsilon \quad (1)$$

where $\Delta\lambda_B$ is the wavelength difference (nm); P_e is the effective bounce coefficient of the grating; λ_B is the wavelength of the center of the light grating (nm); $\Delta\varepsilon$ is the strain change value. K_ε is the sensitivity coefficient (pm/με).

The following expression is the pile axial force during pile jacking.

$$N_i = E_c\Delta\varepsilon A_p \quad (2)$$

where N_i is the pile axial force at the ith FBG sensor position (KN); E_c is the pile concrete modulus of elasticity; $\Delta\varepsilon$ is the variation of the pile strain; A_p is the cross-sectional area of the pile (mm^2)

The following equation stands for the unit frictional resistance on the side of the pile.

$$Q_i = N_i - N_{i+1} Q_i = N_i - N_{i+1} \tag{3}$$

$$q_i = \frac{Q_i}{ul_i} = \frac{N_i - N_{i+1}}{\pi d l_i} \tag{4}$$

where Q_i and q_i is the total and unit lateral friction resistance of section I, respectively; u is the perimeter of the pile; l_i is the distance between section I and i+1, and d is the diameter of the pile cross-section (m).

3.3. Deployment of Fiber-Optic Grating Sensors

Model piles TP1, TP2, and TP3 were attached with six FBG sensors in the outer tube, and the specific deployment steps are as follows.

(1) Measuring and positioning: Using a black water-based pen, mark the pre-installation site of the FBG sensor on piles at the spacing indicated in Figure 4. Number the sensors from the bottom to the top of the pile as 1#–6#.
(2) Slotting: A shallow slot of 2 mm × 2 mm (width × depth) is cut into the surface of the outer tube.
(3) Adhesive sensor: first, paste one end of the fiber grating, clamp both ends of the fiber grating with cotton swabs, then move the unbonded end for pre-stretching; when the wavelength increases around 2 nm, stop pre-stretching, and fix the free end with glue, as shown in Figure 5.
(4) Connect the collector and check the survival rate: After cleaning the sensor's FC connector, connect the collector to the demodulator to check the survival rate. From the results, all of the sensors are alive.
(5) Package protection: the FBG sensor is encapsulated with epoxy resin to flush its surface with the pile surface.

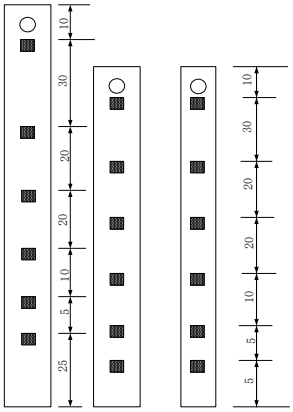

Figure 4. FBG sensor pile layout (unit: cm).

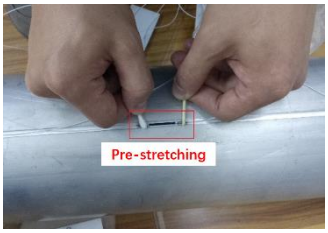

Figure 5. Pre-stretching of FBG sensor.

3.4. Wheel and Spoke Pressure Sensor

In accordance with the test design requirements, the pile tip resistance needs to be measured accurately in this test process to realize the separation of the pile side and tip resistance, so the rotatable wheel-spoke pressure sensor is selected for measurement, as shown in Figure 6.

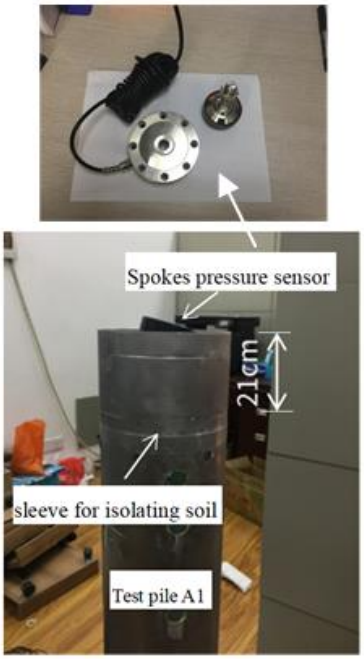

Figure 6. Spoke pressure sensor after installation.

The installation of the spoke pressure sensor is relatively complex; to guarantee the measurement's correctness, the impact of the soil surrounding the pile needs to be reduced, so a soil isolation sleeve was installed to isolate the soil, with a height of about 20 cm. At the beginning of the installation, the soil isolation sleeve is connected to the pile end with inner hexagonal bolts. Then, the pressure sensor was closely linked to the pile end, and the installed sensor was slightly lower than the soil isolation sleeve. Before pile pressing, the bottom end is encapsulated with a steel plate with the same diameter to expand the stress area of the sensor. Both at once, it also guarantees that the sensor's force is uniform. After installation, the spoke pressure sensor is shown in Figure 6. The CF3820 high-speed static signal test analyzer was used to test the survival rate of the sensor. The sensors are all activated, and realize real-time acquisition of the penetration process.

3.5. Brief Introduction of Pile Top Pressure Sensor

From Figure 7, the pile top pressure sensor may satisfy the testing criteria since it has a measuring range of 1 Mpa, a diameter of about 70 mm, and a height of about 25 mm; it was placed horizontally at the pile head before pile jacking, and the real-time test data are collected by fiber Bragg grating demodulator during pile driving.

3.6. Principle of Pile Top Pressure Sensor

During the pile jacking process, the FS2200RM fiber grating demodulator analyzes the wavelength difference to calculate the pile force. After revising the sensitivity coefficient, the pile driving force F is calculated according to Formula (5).

$$\mathrm{F} = \frac{\Delta\lambda_B}{K_\sigma} A \tag{5}$$

In the formula, F is the pile driving force (kN), the $\Delta\lambda_B$ stands for wavelength difference (nm), the K_ε is the sensitivity coefficient (nm/MPa), and A is the cross-section area (mm^2).

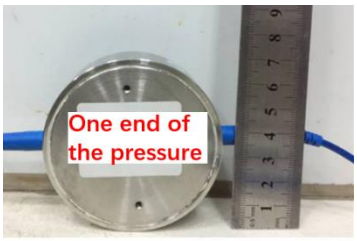

Figure 7. Pile top pressure sensor.

3.7. Installation Guarantee of Test Sensor

The FBG sensor is small and sensitive, so the installation slot should be cleaned with alcohol and a cotton ball before installation; the FC joint is easy to be contaminated, so it should be scrubbed clean with alcohol and a cotton ball before connecting it with the terminal of the demodulator, and then connected to guarantee the measurement's correctness. The pre-stretching of the fiber grating prevents the compressive stress measurement range from being insufficient and increases the compression range. The pressure sensor at the top of the pile is easy to use. Before pressing the pile, it should be aligned with the center of the top of the pile to prevent its eccentricity from causing uneven force in the process of pressing the pile. The FBG sensor test adopts an eight-channel FS2200RM-Rack-Mountable Bragg Meter interrogator, the instrument acquisition frequency is 1 Hz, wavelength resolution is 1 pm, accuracy is 2 pm, working wavelength range is 1500~1600 nm, and dynamic range is ±3 nm.

4. Static Pile-Sinking Test

The static pile model test was conducted about 30 d after the foundation soil preparation was completed to ensure that the foundation was fully consolidated. On the soil samples, indoor geotechnical tests were carried out. The results show that the physical and mechanical properties were up to standard and could be tested in pile jacking. After the preparation of the foundation soil is completed, it is slowly saturated with water in order to accelerate the consolidation of foundation soil.

4.1. Experiment Overview

To guarantee the successful conduct of the experiment and to facilitate the observation of the force state of test piles being jacked, the test design was carried out for a total of three model piles, and the test plan for each test pile is shown in Table 4. The tested piles is shown in Figure 8.

Table 4. Test pile test plan table.

No.	Total Pile Length/mm	Pile Diameter/mm	Form of Pile End	Pile Depth /mm	Pile Driving Speed/(mm/min)	FBG Sensor/Number	Pile Top Pressure Sensor/Number	Pile End Spoke Pressure Transducer/Number
TP1	1200	140	close	1100	300	6	1	1
TP2	1000	140	close	900	300	6	1	none
TP3	1000	100	close	900	300	6	1	none

Figure 8. The tested piles.

4.2. Selection of Pile Position

In this test, two groups of model piles are placed in the middle of the model box, separated from the edge by 1400 mm, and are larger than four times the diameter of the pile. L/D > 10 far exceeds the specifications of L/D > 3 and can ignore the boundary effect [24,25]. The test pile arrangement is depicted in Figure 9.

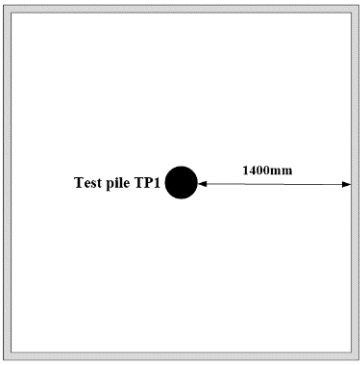

Figure 9. Pile position layout.

4.3. Loading and Measurement of the Test

First, the electronic control system will load the hydraulic jack's beam with the static pile test process before moving it to the designated pile, then open the main chassis through the oil pump control jack up to a certain height. The test pile will be pushed into the upright position to check if the pile is vertical and avoid eccentric pressure; use the magnetic cassette-type leveling tape that has been adsorbed on the pile's surface. Once the pile is upright, pressurize the hydraulic jack once again using the oil pump to cause it to fall gradually and evenly until it reaches the top of the pile and then stops pressurizing. Prior to the formal pile top pressure test, data acquisition is performed by connecting the transmission lines of the pile top and pile side sensors to their respective acquisition devices in turn, verifying that the connections are correct and adjusting the parameters. The test is primarily carried out by pressurizing the jack using an oil pump to cause the static pile to sink, as seen in Figure 10.

Figure 10. Static pile sinking process.

5. Analysis of Static Pile-Sinking Test Results

5.1. Analysis of Force Traits during Pile Sinking

Based on the collected data, a comprehensive study and analysis of the force state of the pile were carried out. Figure 11 shows the full load curves of the three test piles.

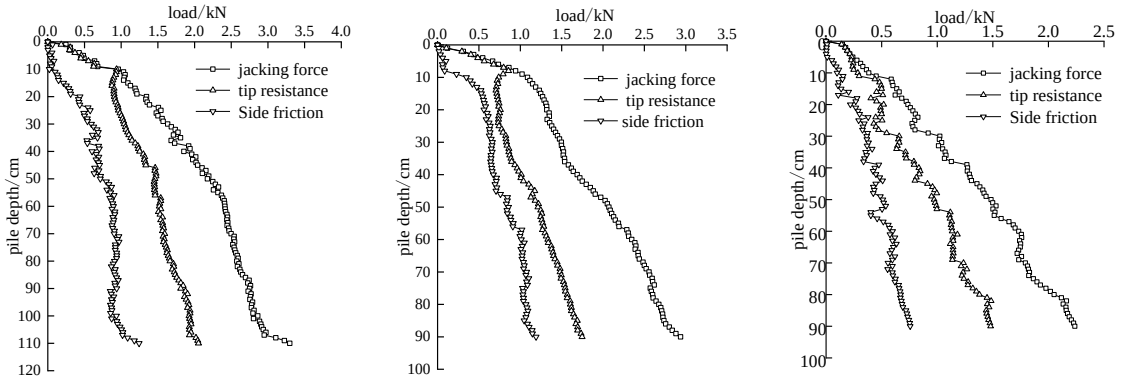

Figure 11. The whole process load curve of each test pile sinking pile. (**a**) Test pile TP1; (**b**) Test pile TP2; (**c**) Test pile TP3.

According to Figure 10, the three test piles' total pile compression force and other loads gradually increased as the embedded depth increased; the trend of the specific parameters of test pile TP1 is similar to TP2 as a whole, but there is a slight change in the values of the two test piles, which is analyzed mainly since both are closed-end piles with the same diameter. The spoke pressure sensor measures the end resistance of test pile TP1, while the 1# FBG sensor approximates the end resistance of pile TP2, and the two piles are different in length, so the readings are also different.

The pile end resistance and pile side resistance as a percentage of the compression force of each test pile can be compiled from Figure 11 and shown in Table 5.

Table 5. Percentage of pile-pushing force at the end of pile sinking.

No.	Jacking Force/kN	Tip Resistance/kN	Percentage/%	Side Friction/kN	Percentage/%
TP1	3.298	2.054	62.3	1.244	37.7
TP2	2.938	1.747	59.5	1.191	40.5
TP3	2.238	1.480	66.2	0.757	33.8

According to the results, the pile end resistance of the three closed test piles exceeded 50% during the pile jacking in cohesive soils, which means that the pile end resistance

carried most of the load. The pile-side frictional resistance did not play its full role, as it accounted for a relatively low percentage of the total pile-driving force.

5.2. Analysis of Piling Force during Pile Sinking

Figure 12 depicts the trend of the compression force with embedment depth during the jacking of the closed-ended pile to see more clearly the effect caused by the variation of pile diameter and length on the load transfer.

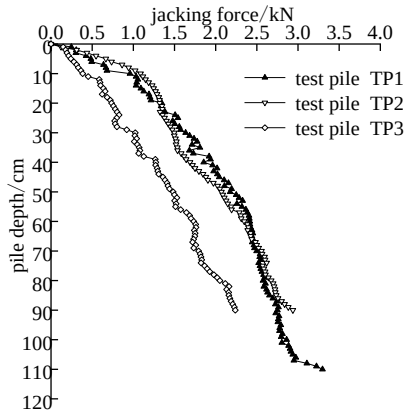

Figure 12. Variation of pile force during static pile sinking.

The compression force of each of the three pipe piles tested rises almost linearly with increasing pile sinking depth. The compression force increases faster when the embedded depth is less than 50 cm. When it exceeds 50 cm, the growth rate decreases significantly, which means that as the sinking depth increases, the soil crowding effect becomes more obvious. The test pile penetration rate into the soil decreases due to the test pile TP3 having a small diameter. As a result, there is little clay-pile contact area and less lateral frictional resistance; the pile end area is small, which results in a small overall pile force. In the sinking depth of less than 23 cm, test pile TP1's piling force is less than TP2, which is attributed to the pile length of test pile TP1 being larger.

Additionally, the contact between the soil and pile was diminished due to the substantial amount of soil disturbance during the first pile sinking. In the sinking depth range of 23 cm to 60 cm, test pile TP1 has a higher piling force than test pile TP2, indicating that the piling force required as the sinking depth rises increases with test pile length. The jacking force of test piles TP1 and TP2 in the 90 cm sinking range is similar. The final jacking force of test pile TP1 is 3.298 kN, which is only 12% higher than the jacking force of test pile TP2; It shows that under the same pile diameter and pile end shape, the pile length has a bigger impact on the pipe pile's final pressure. It demonstrates that when the pile diameter and pile end shape are certain, the pile length has a higher impact on the pipe pile's ultimate pressure. Test pile TP2's final compressive strength was 2.938 kN, while test pile TP3's ultimate pressure was 2.238 kN. According to the findings of the comparison, the ultimate pressure for the test pile with a larger diameter was 31% greater than for the test pile with a smaller diameter, proving that the impact of pile diameter over the ultimate pressure of the submerged pile was greater than that of pile length.

5.3. Analysis of Pile End Resistance during Pile Sinking

The pile end resistance of test pile TP1 was measured by the spoke pressure transducer during static pile sinking, and the pile end resistance of the other test piles was estimated using the lowermost end of pile 1.

From Figure 13, the pile end resistance of the three pipe piles increased gradually with the increased embedded depth during the whole process of pile jacking. The pile end resistance of the three test heaps increases more quickly when the sinking depth is less than

10 cm, and the pile end resistance of test pile TP2 grows fastest at this stage; the analysis may be due to the following reasons: A 20 cm spoke pressure sensor is installed at the end of test pile TP1; however, during the early stages of pile sinking, the sensor is unable to penetrate the soil layer, resulting in minimal pile end resistance. The increasing rate of pile end resistance of the three test piles reduces when the sinking depth exceeds 10 cm, and the relationship between the magnitude of pile force is: test pile TP1 > TP2 > TP3. The reason for this may be that the contact area between the pile and the earth grows as the penetration depth rises, and the pile's lateral resistance rises as a result of pile-to-pile extrusion. The pile's impact on the soil surrounding it is greater, the pile is subjected to more self-weight stress, and the contact area between the pile and soil grows as penetration depth rises. Since the test pile TP1 has a longer pile length and deeper penetration, its influence on the soil around it is greater, such as the greater pile end resistance, which results in the pile end resistance slowing down. After the process of pile jacking, test piles TP1, TP2, and TP3 had a pile end resistance of 2.054, 1.747, and 1.48 kN, respectively. Test pile TP1 was 17.6% higher than TP2, and test pile TP2 was 18% higher than TP3.

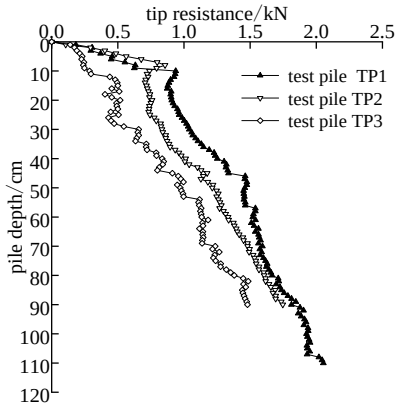

Figure 13. Variation of pile end resistance during static pile sinking.

5.4. Analysis of Pile Side Friction Resistance during Pile Sinking

The calculation of wavelength difference is converted from Equations (1) and (2) and can be used to determine the total pile side resistance during pile jacking (3).

Figure 14 shows that, in general, each test pile's total pile lateral resistance gradually increases with the sinking depth. That is primarily due to the shallow soil body violently shaking as the pile sinks and the pile–soil contact becoming looser because of the protracted soil compacting effect. With regard to the long-time soil compacting effect and the pile–soil contact between a certain gap, contact is no longer close, resulting in the pile–soil adhesion and the soil compacting effect between the basic loss, resulting in the shallow soil body total pile side friction resistance, which is a small phenomenon. Although test pile TP1 has a large embedded depth throughout the pile jacking process, its pile-side resistance is typically dwarfed by the test pile TP2, while the maximum pile-side resistance of test pile TP2 slightly exceeded that of test pile TP1 after jacking. The shearing effect of test pile TP1 on the soil around the pile was more obvious than that of test pile TP2 during pile jacking. As the pore water pressure increases more quickly, a layer of mud film made up of pore water, and debris between the pile and soil becomes thicker. When the mud coating is thicker, pile–soil friction turns into moist friction. The increase in pile side resistance of both test piles slowed down as the piles jacking, and the overall side resistance of test pile TP1 was lower than that of test pile TP2 since the pile–soil friction may produce internal friction when the mud film thickness is larger. At the end of jacking, the side resistance of test pile TP3 was 0.76 kN, while that of TP2 was 1.19 kN, which was 57% larger than that of TP3, indicating that the diameter of the pile had a great influence on the pile side resistance. The larger the pile's diameter, the more its surface area is in contact with the soil around it, and the greater the lateral pressure, the more obvious the jacking process since the compact

soil effect. The pile has a higher side resistance. As a result of the increased lateral pressure, the pile side friction value will also increase. Increasing the pile diameter is more efficient for piles that relying on friction to bear the load.

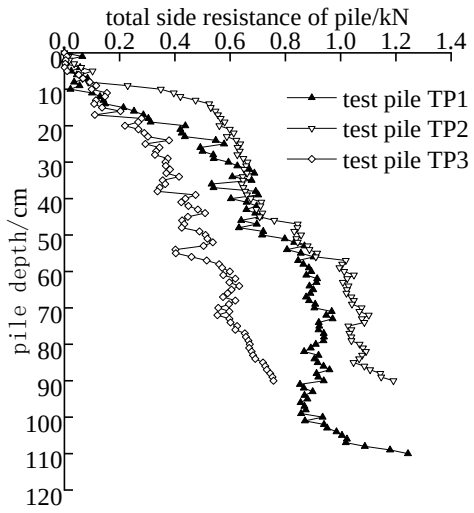

Figure 14. Variation of the side friction of the total pile during static pile driving.

5.5. Analysis of Test Pile Axial Force Results

According to Equations (1) and (2), the graph of pile axial force distribution for the three test piles during jacking are illustrated in Figure 15.

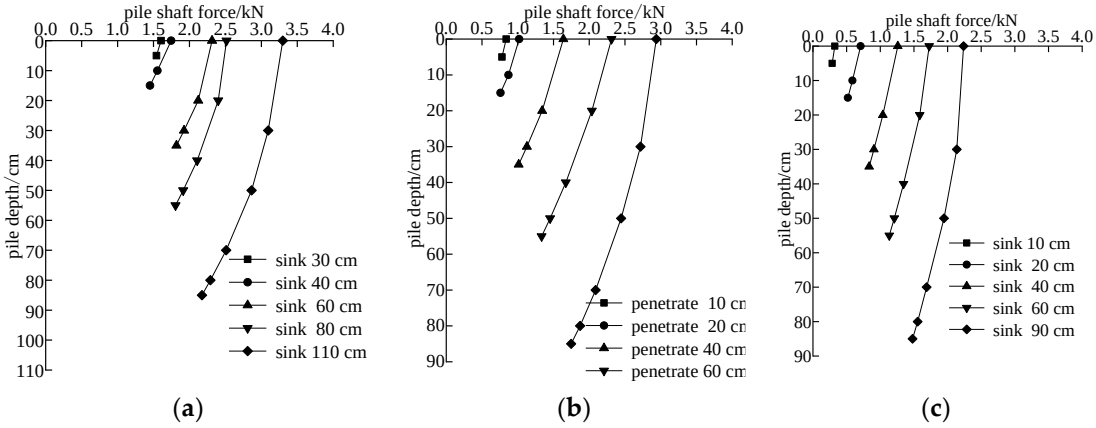

Figure 15. Axial force distribution diagram of test pile body. (**a**) Test pile TP1; (**b**) Test pile TP2; (**c**) Test pile TP3.

According to Figure 15, the test piles TP1 through TP3 have similar pile axial force distributions, meaning that at various penetration depths, the pile axial force decreases as sinking depth increases, and the slope of the curve gradually decreases; the adhesion between soil particles and the pile increases continuously during pile pressing; at this point, the sunken pile requires more shear force to shear the adhesion point, whereas the soil that is tightly adhered to the pile wall produces more extrusion with the soil surrounding the pile, increasing the frictional resistance between the pile and soil. The closer to the lower part of the pipe pile one is, the greater the lateral frictional resistance, and the lower the axial force.

Additionally, when sunk to the same depth, it can be seen from comparing the three test piles that the pile axial force is TP1 > TP2 > TP3. In all three test piles, the shaft force at

the same sinking depth gradually increases with the penetration depth, primarily due to the gradually rising pile compression force.

Figure 15a shows that the difference in pile axial force is very small during the early penetration stages when the plastic deformation of the soil at the pile end has just begun to appear; however, when the penetration has reached 60 cm, the outer pipe axial force suddenly increases, indicating that the soil at the pile end is now aggressively extruded and that its reaction force is higher; when penetrating 80 cm, the increase in axial force is small, which may be the elastic recovery of the part of the soil that has already undergone plastic deformation; when penetrating to 110 cm, the pile axial force showed an increase, which indicates that the soil was re-arranged and crowded, making the foundation harden and the bearing capacity increase extremely quickly.

The pile axial forces of the test piles were 2.174, 1.747, and 1.48 kN, respectively, at the maximum penetration depth. The pile axial force of the test pile TP1 was 24% higher than TP2, and the pile axial force of the test pile TP2 was 24% higher than TP3, indicating that pile length had a greater impact on pile shaft force than pile diameter.

5.6. Analysis of the Results of the Unit Frictional Resistance of the Test Pile Side of the Pile

According to Equations (3) and (4), Figure 16 shows the distribution curve of unit pile-side resistance for each test pile at a certain embedded depth. The vertical coordinate of the unit pile-side resistance corresponding to the section depth used to plot the distribution curve in the figure is the middle of the upper and lower two adjacent FBG sensors.

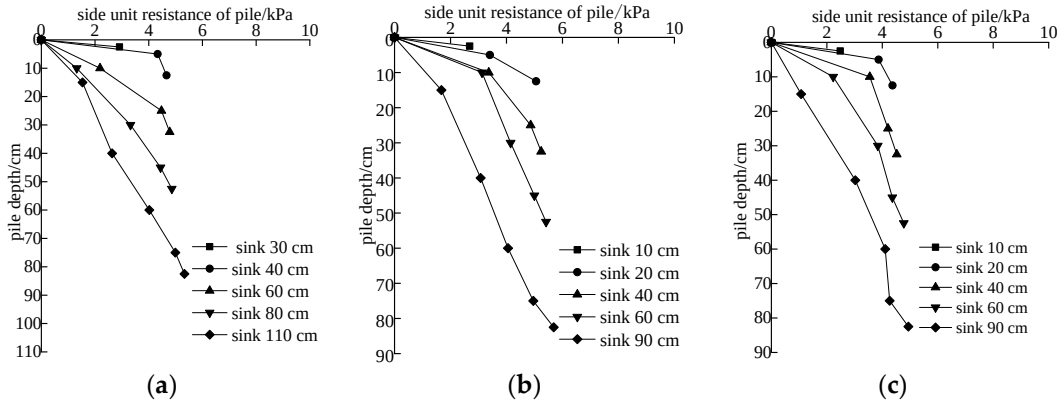

Figure 16. Distribution of side frictional resistance of each test pile body. (**a**) Test pile TP1; (**b**) Test pile TP2; (**c**) Test pile TP3.

Figure 16 shows that for each test pile, the distribution of unit pile-side resistance at various penetration depths is the same, i.e., the pile side resistance has a tendency to build gradually as embedded depth increases, while the growth is not uniform. At the same embedded depth, the unit pile-side resistance progressively declines with pile jacking, i.e., namely, "degradation effect" of pile side resistance [26], and the cause of that is consistent with that put out by Hu [18], i.e., the attachment point between the pile and the soil is cut off more as the penetration depth and duration of repeated plowing increase at the same soil depth. There is no tillage impact, and repeated tillage also increases mud film thickness and releases horizontal tensions, which all contribute to a reduction in lateral frictional resistance. To examine the lateral frictional resistance of pile end 1 at various penetration depths, the test pile TP3 is utilized as an example.

6. Conclusions

The force variation pattern of the pile along the sinking depth was successfully monitored by pre-burying FBG sensors in the pile and inserting pressure sensors at the top of the pile. For the first time, it was suggested to install a 20-cm spoke-type pressure sensor

at the end of the TP1 pile to measure the pile-end resistance, and the test results were encouraging.

The pile diameter had a greater impact on the ultimate pressure of the jacked pile than the pile length. Although test pile TP1 had a spoked pressure sensor installed, the pile-side resistance was only 27.7% higher than that of test pile TP2 with sinking depth increase, but 57% higher than that of test pile TP3 due to the pile diameter, indicating that pile diameter is a significant factor affecting pile lateral frictional resistance.

Each test pile's distribution of pile axial force at various penetration depths is comparable; the pile axial force continually drops as the pile jacking, and the slope of the distribution curve of axial force gradually lowers. The axial forces of test piles TP1 and TP2 are 24% and 18% higher at the end of jacking, respectively, demonstrating that the pile length more strongly influences the pile axial force than the pile diameter.

In the static pile sinking process of three test piles in cohesive soil, 50% is end bearing; therefore, there is 50% friction, and the diameter influences the end bearing and the length influences the friction.

The authors only conducted a single test for each type of pile. Comparative tests of the same type of pile are missing. The preparation of soil samples in this test is very complicated, and some meaningful conclusions have been obtained by changing the pile diameter and pile length, and the comparative tests of each test pile will be supplemented in the follow-up trials.

Author Contributions: Conceptualization: L.W., Y.W.; Data curation: S.Z., Y.W.; Funding acquisition: Y.W.; Project administration: S.L., J.W., X.N.; Writing—original draft: L.W., S.Z., D.W.; Writing—review and editing: S.L., J.W., X.N., D.W., Y.W. All authors have read and agreed to the published version of the manuscript.

Funding: This work was supported by the National key research and development plan (2021YFE0113400), the Shandong National Natural Science Foundation (ZR2022ME143).

Data Availability Statement: The experimental data used to support the findings of this study will be made available upon request.

Conflicts of Interest: The authors declare that there are no conflict of interest regarding the publication of this paper.

References

1. Liu, J.W. *Study Pile Driving Process and Static Pressure Pile Bearing Capacity*; Qingdao University of Technology: Qingdao, China, 2008.
2. Murthy, D.S.; Robinson, R.G.; Rajagopal, K. Formation of soil plug in open-ended pipe piles in sandy soils. *Int. J. Geotech. Eng.* **2018**, *15*, 519–529. [CrossRef]
3. Li, J.P.; Li, L.; Sun, D.A.; Tang, J.H. Theoretical study on sinking resistance of jacked piles in saturated soft clay. *Chin. J. Geotech. Eng.* **2015**, *37*, 1454–1461. [CrossRef]
4. Sagaseta, C.; Whittle, A.J.; Santagata, M. Deformation analysis of shallow penetration in clay. *Int. J. Numer. Anal. Methods Geomech.* **1997**, *21*, 687–719. [CrossRef]
5. Zhang, M.Y.; Deng, A.F. Experimental study on jacked precast piles in layered soil. *Chin. J. Geotech. Eng.* **2000**, *22*, 490–492. [CrossRef]
6. Ma, H.L. Field test on time effect of bearing capacity on end-open pile and end-closed pile. *Chin. J. Rock Mech. Eng.* **2008**, *27*, 3349–3353. [CrossRef]
7. Kou, H.L.; Zhang, M.Y.; Liu, J.W. Bearing capacity efficiency mechanism analysis of jacked pile based on optical fiber sensing technology. *Rock Soil Mech.* **2013**, *34*, 1082–1088. [CrossRef]
8. Kou, H.L.; Zhang, M.Y. Penetration mechanism of jacked PHC pipe piles based on pile stress measurement. *Rock Soil Mech.* **2014**, *35*, 1295–1302. [CrossRef]
9. Li, Y.N.; Barry, M.L.; Liu, Q.B. Centrifuge modeling of jacked pile in clay. *Chin. J. Eng.* **2018**, *40*, 285–292. [CrossRef]
10. Nicola, A.D.E.; Randolph, M.F. Centrifuge modelling of pipe piles in sand under axial loads. *Geotechnique* **1999**, *49*, 295–318. [CrossRef]
11. Hassan, N.S.; Ibrahim, A.; Alias, R.; Hasbollah, D.Z.A.; Ramli, A.B. Assessment of ultimate bearing capacity of the pile for jacking & rotary piling method. *Phys. Chem. Earth* **2023**, *129*, 103331.

12. Lee, C.Y.; Poulous, H.G. Jacked model pile shafts in offshore calcareous soils. *Mar. Georesour. Geotechnol.* **1988**, *7*, 247–274. [CrossRef]
13. Statkus, T.; Norkus, A.; Mikolainis, M. Experimental Investigation of Settlement in Sand Soil of Jacked Pile Subjected by Vertical Compressive Cyclic Loading. *Procedia Eng.* **2017**, *172*, 1053–1058. [CrossRef]
14. Wang, Y.; Li, J.; Li, L. Settlement of jacked piles in clay: Theoretical analysis considering soil aging. *Comput. Geotech.* **2020**, *122*, 103504. [CrossRef]
15. Yang, Q.G.; Liu, J.; He, J.; Luo, S.H. Comparative research on penetration resistance of jacked tapered piles and uniform section piles. *Chin. J. Geotech. Eng.* **2013**, *37*, 897–901.
16. Gu, H.W.; Kong, G.Q.; Che, P.; Ren, L.W.; Peng, H.F. Comparative model tests on bearing capacities of tapered pile and equal section pile. *J. Cent. South Univ. (Sci. Technol.)* **2017**, 194–200.
17. Kou, H.L.; Li, W.; Chu, J.; Yang, D.L. Model tests on open-ended concrete pipe piles jacked in sand. *Mar. Georesour. Geotechnol.* **2019**, *38*, 939–946. [CrossRef]
18. Hu, Y.Q.; Tang, L.S.; Li, Z.Z. Experimental Study on Variation and Time Effect of Shaft Resistance of Jacked Pile Installation. *Acta Sci. Nat. Univ. Sunyatseni* **2015**, *54*, 130–135. [CrossRef]
19. Li, Y.; Zhu, W.; Zheng, W.; He, J. Surrounding rock mass stability monitoring of underground caverns in a geomechanical model test using FBG sensors. In Proceedings of the Second International Conference on Smart Materials and Nanotechnology in Engineering, Weihai, China, 8–11 July 2009; p. 7493.
20. You, R.; Ren, L.; Song, G. A novel fiber Bragg grating (FBG) soil strain sensor. *Measurement* **2019**, *139*, 85–91. [CrossRef]
21. Zhu, Y.Q.; Zhu, H.H.; Sun, Y.J.; Shi, B. Model experiment study of pipe pile driving into soil using FBG-BOTDA sensing monitoring technology. *Rock Soil Mech.* **2014**, *35*, 695–702. [CrossRef]
22. *GB/T 50123-1999*; Industry Standard Compilation Group of the People's Republic of China. Standard for Geotechnical Test Methods. China Planning Press: Beijing, China, 1999.
23. *JGJ 94-2008*; Technical Specifications for Building Pile Foundations. Technical Code for Building Pile Foundation. China Building and Building Press: Beijing, China, 2008.
24. Ovesen, N.K. The scaling law relationship-Panel Discussion. In Proceedings of the 7th European Conference on Soil Mechanics and Foundation Engineering, Brighton, UK, September 1979; pp. 319–323.
25. Xu, G.M.; Zhang, W.M. Study on particle size effect and boundary effect in centrifugal model. *Chin. J. Geotech. Eng.* **1996**, *18*, 80–86.
26. Liu, J.W.; Zhang, M.Y.; Yu, F.; Bai, X.Y. Experimental study on interface shear fatigue between soils and PHC pipe piles. *Chin. J. Geotech. Eng.* **2013**, *34*, 1037–1040.